Pure appl. geophys. 158 (2001) 259–276
0033–4553/01/000000–00 $ 1.50 + 0.20/0

Pure and Applied Geophysics

Best Practice in Earthquake Location Using Broadband Three-component Seismic Waveform Data

ROBERT A. UHRHAMMER,[1] DOUGLAS DREGER[1] and BARBARA ROMANOWICZ[1]

Abstract — We present an earthquake location algorithm, the Broadband Waveform Regional Earthquake Location Program (*BW_RELP*), which utilizes phase onset times and wave azimuths recorded by three-component broadband seismic stations and an adaptive migrating grid search algorithm to find the global minimum in an arbitrary normed misfit parameter. The performance of *BW_RELP* is demonstrated using regional (300–800 km distant) broadband recordings to locate events in the 1995 Ridgecrest, California earthquake sequence. The purpose of this study is to introduce the *BW_RELP* algorithm in detail and to expand on the previous paper by DREGER *et al*. (BSSA, *88*, 1353–1362, 1998), using one Berkeley Digital Seismic Network (BDSN) station (YBH) and two USNSN stations (ELK and MNV) which span 300–800 km in distance and 55 degrees in azimuth, to further investigate the capability of a sparse broadband network of three-component stations at monitoring a region located outside of the network, as will be the case in the monitoring of the Comprehensive Test-Ban-Treaty (CTBT) for low magnitude seismic events. We assess the capability of this sparse three-station broadband network and we compare locations estimated from phase onset time and wave azimuth measurements to a ground-truth catalog of high-quality earthquake locations derived from data recorded by the Southern California Seismic Network (SCSN). The results indicate that in the regional distance range it is possible, when an appropriate calibration event is available, to obtain absolute event locations to within 18 km as is prescribed by the CTBT.

Key words: Broadband network, three-component stations, earthquake location algorithm, CTBT.

Introduction

Most conventional earthquake location algorithms in widespread use by the seismological community (i.e., LEE and LAHR, 1972) use phase onset time data and some variant of Geiger's method (GEIGER, 1910) in which a linearized inversion process is iteratively solved until a convergence criteria is satisfied. These linearization algorithms generally suffer from two fundamental limitations: they make limited use of the information inherent in seismic wavefield recordings obtained from modern three-component broadband seismometers coupled to high-resolution digital data loggers, and they implicitly assume that the error surface is ellipsoidal (GEIGER, 1910; FLINN, 1965). We take advantage of the additional information inherent in

[1] Berkeley Seismological Laboratory, University of California, Berkeley, CA 94720-4760, U.S.A.

these broadband recordings by measuring the wave azimuth as well as the phase onset time for use in locating the seismic source. The wave azimuth data are complimentary to the phase onset data and their combined use results in more robust solutions. Direct mapping of the iso-misfit surface shows that it is generally asymmetrical and not ellipsoidal in shape (BULAND, 1976). The inherent assumption that the error surface is ellipsoidal can lead to significant systematic errors in the estimated uncertainties. We introduce a recently developed earthquake location algorithm, the *Broadband Waveform Regional Earthquake Location Program* (*BW_RELP*), which does not suffer from the above limitations and which was specifically designed for the problem of locating earthquakes when the available data are from a sparse broadband network and when the source region is outside of the network. Our motivation was, in part, to develop a robust algorithm for locating earthquakes in California and vicinity when the only available data was from a few Berkeley Digital Seismic Network (BDSN) broadband stations. *BW_RELP* uses both phase onset time and wave azimuth data and an adaptive migrating grid search algorithm to find the minimum in an arbitrarily normed misfit parameter space. The corresponding uncertainties are determined by direct mapping in the misfit parameter space.

The recent proliferation of broadband seismic station networks, such as BDSN, offers the opportunity to analyze seismic events over a wide range of seismic moment release. This will likely be the case in the monitoring of the Comprehensive Test-Ban-Treaty (CTBT) using the International Seismic Monitoring System (ISMS) for small magnitude events, and for studying earthquakes in the United States using the National Seismic Network (NSN). Sparse broadband networks have been deployed in northern and southern California (BDSN and TERRAscope, respectively), in the Mediterranean (MedNet), in Japan (FREESIA NET), in the continental US (USGS NSN), and on a global scale (IRIS GSN). Stations from these networks contribute to the International Seismic Monitoring System (ISMS). A key design consideration for the Primary and Auxiliary seismic networks of the ISMS was that these networks be capable of locating $M \geq 4$ events with an uncertainty of less than 1000 km^2, i.e., within a circle of radius less than 18 km. For low-yield explosions or evasively tested nuclear devices the resulting small magnitudes will preclude the recording of signals from IMS stations at teleseismic distances, and will necessarily focus the analysis effort on distances of a few hundred to perhaps 2000 km, where lateral heterogeneity in earth structure significantly complicates the problem.

The purpose of this paper is to describe the *BW_RELP* algorithm and to expand on our study (DREGER *et al.*, 1997) which evaluated the effectiveness of a sparse broadband network for monitoring a region. The 1995 M_L 5.8 Ridgecrest, California earthquake sequence (Fig. 1; Table 1) is ideally suited for this study because the events were located employing a local seismic network, because the energetic sequence produced numerous aftershocks $M_L \geq 3.5$, and owing to very compact the source region. The Ridgecrest sequence events studied here are given in Table 1

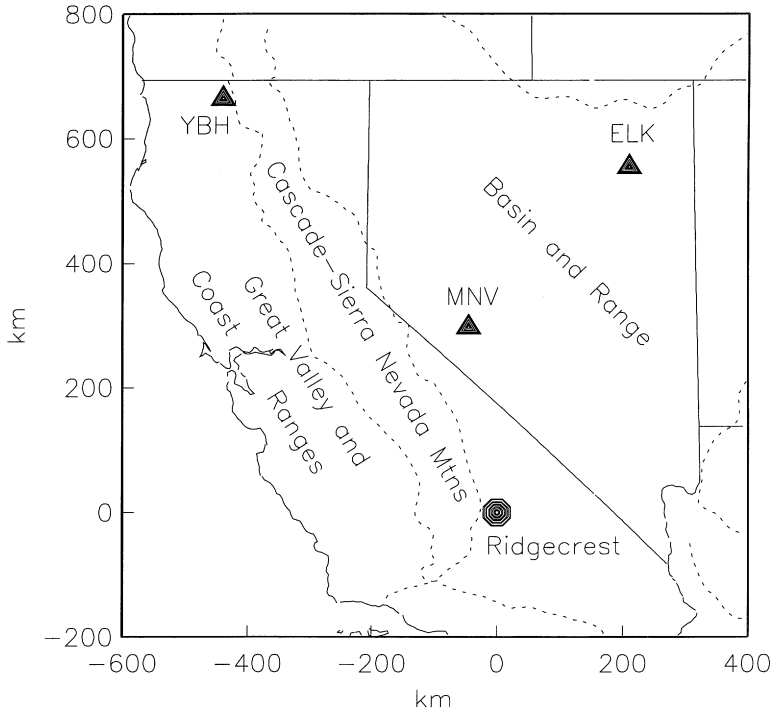

Figure 1
Map showing the locations of BDSN station at Yreka, California (YBH), the USNSN stations in Mina, Nevada (MNV) and Elko, Nevada (ELK), the location of the 1995 Ridgecrest sequence, and the Physiographic Provinces. The Ridgecrest sequence "ground-truth" locations all plot within a circle one-fifth the diameter of the octagon. There is considerable variation in the physiological structure along the propagation paths to the three stations as indicated by the dashed lines that outline the Great Valley and Coast Ranges, the Cascade-Sierra Nevada Mtns, and the Basin and Range Provinces.

where the locations, adopted as "ground truth" for comparison purposes, were determined using data from the local Southern California Seismic Network (SCSN). All the hypocenters in Table 1 fit within a 4-km-radius sphere so the source region for the M_L 5.8 sequence is unusually compact. A compact source region is advantageous when comparing the broadband waveforms and picking phase onset times because the absolute travel times to any one station vary only by approximately ± 1 second between events.

We also discuss modifications to standard processing techniques which can improve performance. The location analysis is evaluated using one Berkeley Digital Seismic Network (BDSN) station located in northern California (YBH, an auxiliary IMS station) and two USNSN stations (ELK and MNV) located in Nevada (see Fig. 1), which span 300–800 km in distance and 55 degrees in azimuth, to further investigate the capability of a sparse broadband network of three-component stations to monitor a region located outside of the network.

Table 1

1995 Ridgecrest sequence locations

Event #	Date	Time	Lat.	Long.	Depth	M_L
1	1995/08/17	22:39:58.99	35.776	−117.662	5.55	5.4
2	1995/08/30	15:29:54.62	35.791	−117.641	4.96	4.2
3	1995/08/30	15:54:22.46	35.796	−117.640	3.36	4.0
4	1995/08/31	01:58:58.78	35.793	−117.644	5.15	3.9
5	1995/09/11	18:37:23.75	35.788	−117.663	6.61	4.2
6	1995/09/20	23:27:36.27	35.761	−117.638	5.42	5.8
7	1995/09/20	23:56:58.50	35.781	−117.666	5.32	3.9
8	1995/09/21	07:46:53.65	35.759	−117.637	5.09	3.9
9	1995/09/21	07:57:41.34	35.756	−117.633	5.38	4.0
10	1995/09/21	23:48:39.16	35.761	−117.643	5.44	4.0
11	1995/09/24	13:15:30.04	35.791	−117.660	6.34	3.7
12	1995/10/06	19:15:04.26	35.758	−117.636	5.40	3.6
13	1995/10/11	14:45:35.14	35.799	−117.633	5.13	3.5
14	1996/01/07	14:32:53.06	35.766	−117.649	5.90	5.2

Earthquake Location Algorithm

To improve the sparse network locations, a new algorithm, herein referred to as *BW_RELP*, was developed to make use of multiple phase onset times and wave azimuth information (DREGER *et al.*, 1996, 1997). The algorithm was specifically designed with the goal of providing robust earthquake locations under adverse conditions during which conventional algorithms fail. As such, we drew on a combination of methodologies to avoid the known limitations of conventional algorithms, to utilize more of the information inherent in broadband seismic records, and to develop a "best practice" algorithm. The major components of the *BW_RELP* algorithm are described in the following paragraphs. The reader is referred to the Berkeley Seismological Laboratory (BSL) web page (URL given below) for more detail.

BW_RELP finds the location of the event by searching for the global minimum in a misfit function in which the misfit is a measure of the difference between the observed and the calculated data. The algorithm is designed to utilize both phase onset time and wave azimuth data to locate the event. Since phase onset time (in seconds) and wave azimuth (in degrees) are not in the same units, we cast both the time residuals and the azimuth residuals in terms of a distance metric. The misfit function that is used in *BW_RELP* is:

$$P = \sum_{i=1}^{n} \left(\sqrt{(1-\alpha)(\delta r)^2/n_t + \alpha(\Delta\delta\varphi)^2/n_\varphi} \right)^{\text{norm}}, \tag{1}$$

where P is the misfit value; α is a parameter which provides relative weighting between travel time and wave azimuth data; δr is the travel-time residual which is

cast in terms of a distance metric where $\delta r = \delta t^* v$ (where δt is the travel-time residual and v is the wave velocity); $\Delta\delta\varphi$ is the azimuth residual which is also cast in terms of a distance metric in the form of an arc length (where $\delta\varphi$ is the azimuth residual and Δ is the distance to a station); and n_t and n_φ are the number of time picks and azimuth picks, respectively. The misfit function utilizes only travel time information if $\alpha = 0$ and only azimuth information if $\alpha = 1$ and a typical value for α is $\sim$0.1. The wave velocity (v) is set to an average wave velocity, typically $\sim$6 km/s. The norm value can range between 0 and ∞. However, there is no compelling reason for using norm values larger than the least-squares value of 2. In practice, the preferred norm value is one which closely matches the observed distribution of the residuals. Empirically, we find that a value of 1.25, as suggested by KENNETT (1996), provides a good match to the residual distribution and also robust solutions. The summation in equation (1) is performed for n phase readings where the phase readings can be either wave arrival time(s) or wave azimuth(s). The algorithm can support any number of phase readings from a single station. Empirically, we have found that using both travel time and wave azimuth data, and 1-D velocity models in the forward calculations, has the added advantage that the misfit function (P) is very robust in that it has only a global minimum and no local minima. One might expect this to be the case since the time and azimuth distance metrics used in constructing the misfit parameter are approximately orthogonal to each other.

In lieu of an inverse approach, a grid search technique (SAMBRIDGE and KENNETT, 1986) is used to locate the minimum in the misfit function. This approach provides a level of flexibility that would be difficult to achieve with a standard inverse approach and does not suffer from the numerical instabilities found in inverse algorithms (BULAND, 1976). In *BW_RELP*, the grid searching algorithm is both adaptive and migratory. The grid search parameters are set by the user to control the starting grid extent, the mesh size, the migration rate, the shrinkage rate of the four-dimensional grid (origin time, latitude, longitude, and depth), and the convergence criteria. The grid search algorithm is adaptive in the sense that the grid migrates and shrinks as it converges on the minimum in the misfit parameter in the four-dimensional parameter space. Figure 2 shows an example of how the adaptive grid search procedure converges. The grid migrates if the minimum in the misfit function is near the edge of the grid and shrinks if it is near the center of the grid. The process continues until both the successive iteration step size and the grid mesh size are both smaller than the size of the convergence parameter. This approach has been found to be both robust and efficient. The adaptive grid search is also more amenable to the incorporation of 3-D velocity models because it is not necessary to compute complicated partial derivatives.

In inverse location algorithms, the quality of the solution is typically indicated by an error ellipsoid whose size is determined using a first-order Taylor series expansion approach to map the solution variance from the data variance (GEIGER, 1910; FLINN, 1965). This approach is not ideally suited for analyzing sparse network data

using *BW_RELP* because it requires the calculation of derivatives and for the reason that it implicitly assumes that the error surface is an ellipsoid and that the number of observations is large. The problem at hand is to determine the size and shape of the iso-misfit surface in the misfit parameter space which represents a desired level of confidence (one standard deviation or the 95% confidence level, namely) in the location of the event. BULAND (1976) investigated mapping of the error surface and demonstrated that when the volume of the parameter space in which the linear approximation is valid is sufficiently large, the uncertainty corresponding to given iso-misfit value may be simply calculated using a χ^2 statistic, and his numerical example using 4 stations and 8 travel-time observations indicated that a 99% confidence error could be calculated reliably. TARANTOLA and VALETTE (1982) also provide a detailed description of mapping uncertainties in inherently nonlinear problems. The approach used in *BW_RELP*, to estimate the size and shape of the iso-misfit error surface at a desired confidence level (one standard deviation, say), is to determine (in sequential order) the standard error of the residuals (δr and $\Delta\delta\varphi$ in Equation (1)), the equivalent origin time standard error, the average of the iso-misfit

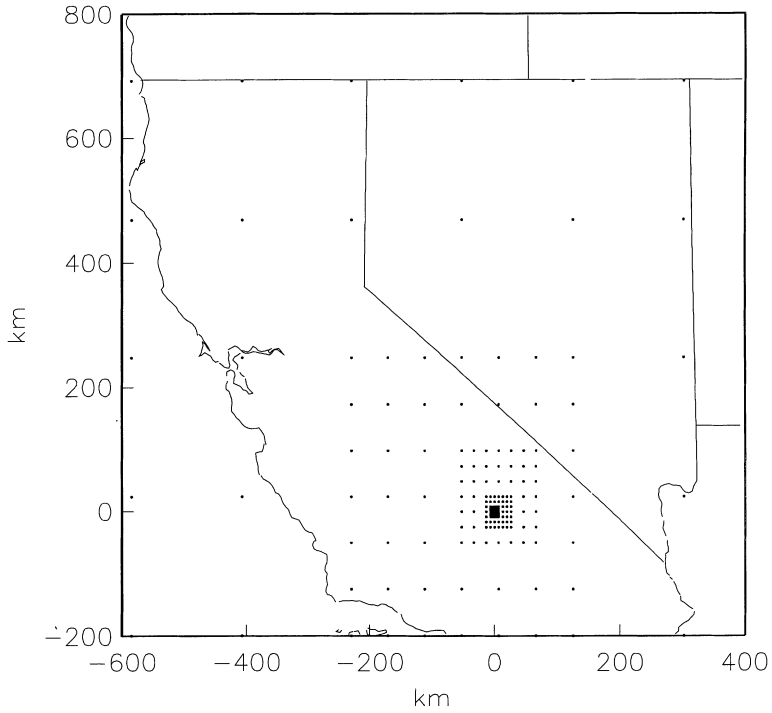

Figure 2
Example of an adaptive grid search. The dots designate the specific locations that were tested. The grid shifts and contracts as the method converges. The "ground-truth" location is at 0 km on both axes. The grid converged to within a km of the final solution in 5 iterations.

value corresponding to perturbations of ± 1 standard deviation in the origin time around the global minimum solution, and finally to determine the corresponding uncertainties in the latitude, longitude, and depth. Actually the confidence level, at which the uncertainties in the solution are calculated in *BW_RELP*, is a parameter that is set by the user. Several tests have been performed comparing the size and shape of the error surfaces calculated by *BW_RELP* and by a convention inversion algorithm (for equivalent and well-determined least-squares problems using only travel-time data), and they produced uncertainty estimates that differed by less than 5 percent. An example of the horizontal projection of error surfaces corresponding to various levels of confidence is shown in Figure 3.

The *BW_RELP* algorithm, man pages, and representative examples are available online via the BSL home page via URL http://www.seismo.*berkeley.edu*/*seismo*/*algorithms*. The default model for the calculation of travel times and azimuths is a gradient layer over a half space where the model parameters are user-supplied. For a more complex model, the user must supply the appropriate travel time and azimuth calculation algorithms. *BW_RELP* is written in FORTRAN, however any

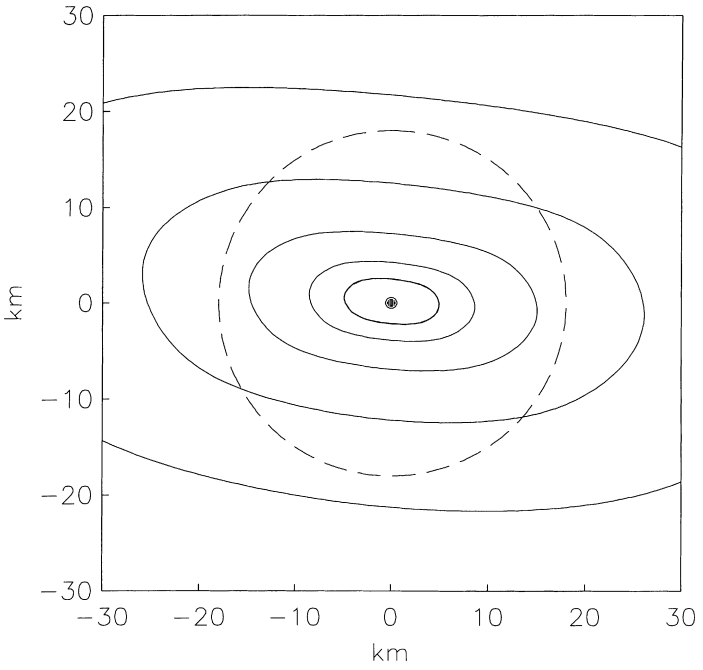

Figure 3
Example of mapping the P_{95} region for Event #1 in Table 1. The misfit parameter was determined every 1 km on a grid, and the resulting values were contoured. The innermost contour represents the P_{95} region (2 standard deviations) and the remaining contours represent 4, 8, 16, and 32 standard deviations. The general shape of the contours reflects the sparse broadband network geometry. The circular dashed line is the prescribed CTBT 1000 km^2 area (18 km radius). The solid circle is the ground-truth location.

user-supplied forward model calculation algorithms need not be restricted to that programming language. There are no default parameters in the algorithm and that all parameters must be set by the user. This was intentionally done for flexibility in the algorithm and because appropriate parameter values are not necessarily known *a priori*. A local event is used to facilitate a comparison of the solutions obtained from the *BW_RELP* algorithm and from standard inversion algorithms. A comparison of the uncertainty volumes determined using *BW_RELP* and a conventional inversion algorithm is included.

Analysis of Sparse Broadband Station Event Locations

The locations of the three regional broadband stations and the Ridgecrest events used in this study are shown in Figure 1. To demonstrate the capabilities of the *BW_RELP* algorithm at far-regional distances, we purposely chose the BDSN station YBH in northern California, as it has been designated as an Auxiliary International Monitoring System (IMS) station, and the two USNSN broadband stations in Nevada (ELK and MNV) to provide azimuth coverage of the source region. These three stations span ~300–800 km in distance and ~55 degrees in azimuth relative to the earthquakes.

There are two fundamental impediments to determining accurate absolute epicenter locations when analyzing events that are at regional distances and external to a sparse broadband seismic network. First, the propagation paths can be quite complex if a variety of physiographic provinces are traversed by the seismic waves. The propagation paths from Ridgecrest to the sparse three-station broadband network happens to be rather complex, as shown in Figure 1, and the use of inadequate velocity models can easily lead to systematic location errors in excess of 100 km (DREGER *et al.*, 1997). Second, consistent picking of the phase onset times and wave azimuths become problematic at large distances and at small magnitude, owing to the degradation in the broadband signal-to-noise ratio (SNR). Appropriate passband filtration of the broadband signals to maximize the SNR, combined with cross-correlation methodologies, significantly enhances the determination of relative phase arrival times and wave azimuths. If an appropriate calibration event with an accurately known location is available, these impediments can be abated since the calibration event can be used both as a template for phase arrival and wave azimuth measurements and as a model calibrator to provide high accuracy relative locations. If no appropriate calibration event is available, one must resort to the daunting task of determining a velocity model with sufficient accuracy to reduce the systematic errors to an acceptable level. In the following sections we use the largest event in the Ridgecrest sequence (M_L 5.8; event #6 in Table 1) as a calibration event for determining the locations of the remaining events in the sequence.

Broadband Waveform SNR

As an example of the large SNR variation with earthquake magnitude that is encountered at regional distances, we display the raw broadband waveforms recorded at YBH (800 km from Ridgecrest) in Figure 4. Note that many of the events are not easily discernible to the eye when viewing the raw broadband data. Figure 5 shows the P-wave and S-wave SNR for the largest event in the Ridgecrest sequence (M_L 5.8) recorded at YBH. The P-wave SNR is highest in the 0.3–4 Hz

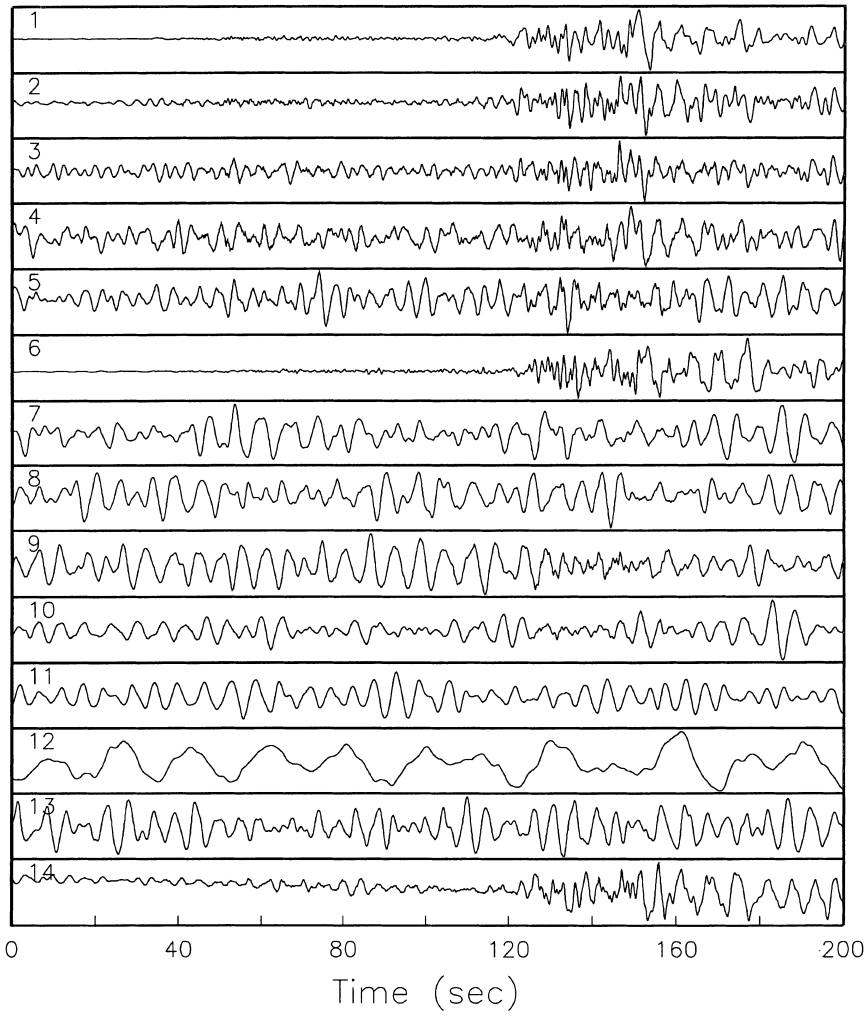

Figure 4
The raw BHZ waveforms recorded at YBH for the 23 Ridgecrest events in Table 1. Note that the smaller events are not readily discernible and filtration is required prior to reading the seismic phases onsets and wave azimuths. The trace numbers correspond to the event numbers in Table 1.

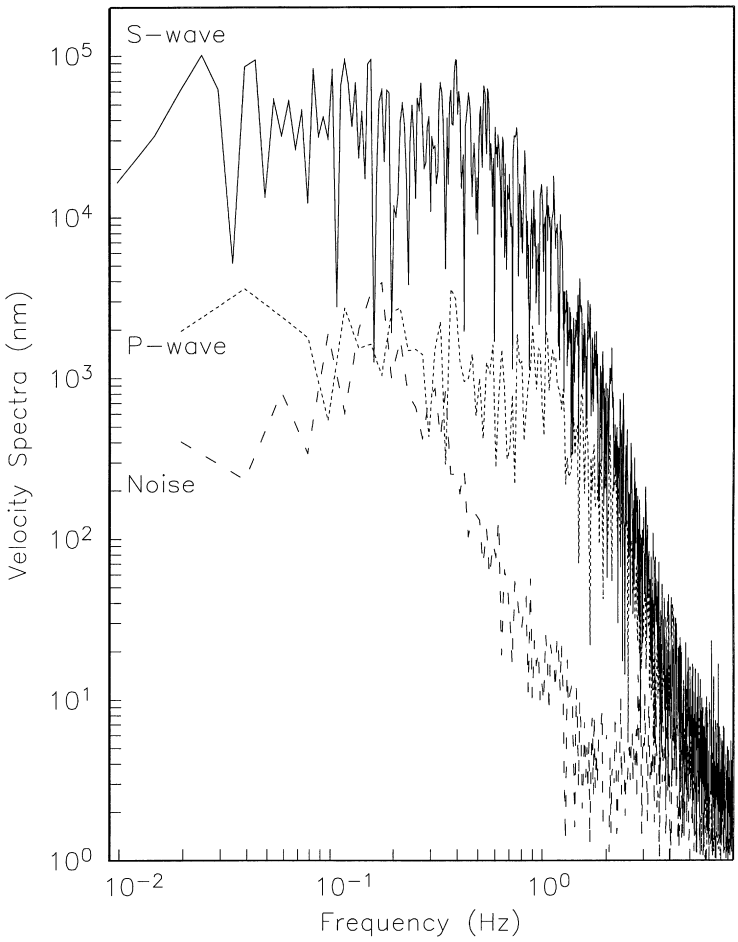

Figure 5
Velocity spectra of the P wave and S wave for the largest Ridgecrest earthquake (M_L 5.8). At 800 km from the source, the signal is below the noise level for frequencies above 4 Hz and the S-wave signal is about 30 dB above the P-wave signal at frequencies below ~0.5 Hz.

passband, it is ~40+ dB in the 1–2 Hz passband and it degrades to ~0 dB at approximately M_L 3.8. The S-wave SNR is 30+ dB in the 0.02–4 Hz passband and 40+ dB in the 0.6–2 Hz passband; the SNR degrades to ~0 dB below 0.3 Hz at approximately M_L 4.3 and it degrades to ~0 dB in the 0.6–2 Hz passband at approximately M_L 3.8. Assuming that a minimum SNR of ~6 dB is required to consistently pick phases, we will be unable to reliably pick the P- and S-wave phase data at YBH for Ridgecrest events smaller than M_L ~4.1. Reliably determining wave azimuths to a precision of order 1 degree requires an SNR of approximately 12 dB or better within an appropriate passband on the radial component relative to the

transverse component (assuming that a 5 second window is used to determine the azimuth). This implies that the wave azimuth recorded at YBH will not be well resolved for Ridgecrest earthquakes smaller than approximately M_L 4.5. Similar analyses for ELK (~600 km from Ridgecrest) and MNV (~300 km from Ridgecrest) indicate that corresponding M_L thresholds are ~0.4 and ~1.4 lower than the values for YBH, respectively. The active tectonic region of the Western US has relatively high seismic wave attenuation and in other regions of the world, where the seismic wave attenuation is lower, the M_L threshold will be correspondingly reduced.

Determination of Phase Arrival Times

We show in detail the process of picking the P-wave phase arrival times for only YBH as it is the most distant of the three broadband stations and it has the lowest SNR. The other two broadband stations (ELK and MNV) were analyzed in a similar fashion. Owing to the large SNR variation observed in the YBH three-component broadband waveforms, and based on the spectral analysis conducted above, we passband filtered the P-wave portion of the waveforms using a six-pole Butterworth filter with a 0.6–2 Hz passband, resulting as shown in Figure 6. Note that the P-wave onset is not easily discernible for many of the events and that there are secondary P-wave arrivals that are readily apparent for all except the smallest events. Consequently, we chose to determine the times of the secondary P-wave arrival for use in determining the location of the events. We used the maximum in the cross-correlation over a 5 second time window to determine the relative arrival time of this phase for each event to an accuracy of approximately ± 25 ms for all except the smallest events. Some of the cross-correlation maxima were negative, owing to differences in the source mechanisms (DREGER *et al.*, 1997). The arrival times of the S wave at YBH were calculated in a like fashion. The arrival time results for all three broadband stations are shown in Table 2.

Determination of Wave Azimuth

As was the case with travel time, we show in detail the process for determining the wave azimuth for only YBH as it is the most distant of the three broadband stations and it has the lowest SNR. The other two broadband stations were analyzed in a similar fashion. We used the same filtered waveforms as in the above section. To determine the wave azimuth we search for the azimuth θ which maximizes the correlation function:

$$c(\theta) = \frac{\sum_{j=1}^{m} (Z_j(N_j \cos(\theta) + E_j \sin(\theta))}{\sum_{j=1}^{m} (E_j \cos(\theta) - N_j \sin(\theta))^2} \tag{2}$$

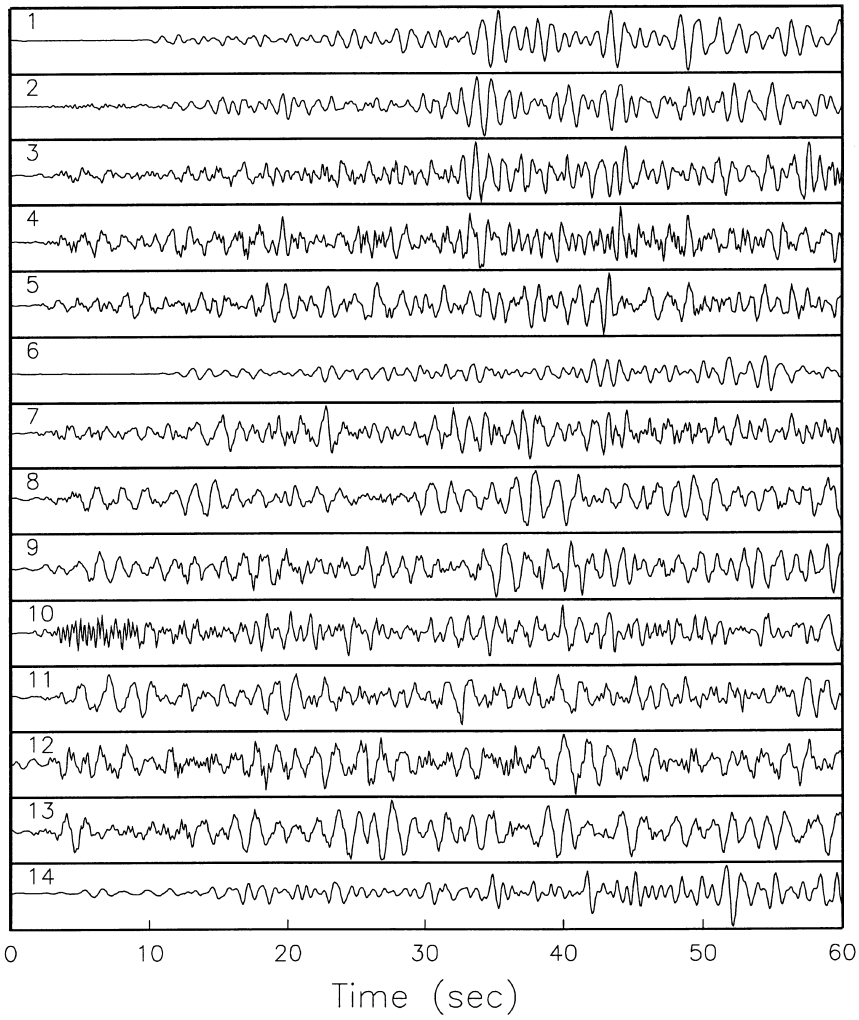

Figure 6
P-wave filtered (6PBP at 0.3–4 Hz) *Z*-component waveforms recorded at YBH, The secondary P-wave arrival at circa 42–44 seconds was chosen for reading as it was visible to all except the smallest M_L events. The numbers on the traces correspond to the event numbers in Table 1.

where Z_i, N_i, and E_i are the vertical, north, and east components, respectively, of the filtered broadband ground velocity at time i. The uncertainty in θ is approximately 0.5 degree for the larger earthquakes and it degrades rapidly when the SNR is below approximately 12 dB as estimated in the SNR section above. The wave azimuth results for all three broadband stations are shown in Table 2.

Locating Ridgecrest events using only phase picks and a standard travel-time inverse procedure without adjustments were found to have large absolute misloca-

Table 2

Observed phase arrival times and wave azimuths

Station	MNV	ELK	YBH
Distance (km)	300.1	591.4	796.4
Azimuth (deg)	351.19	19.98	327.87
P Travel time (sec)	50.464	110.393	148.295
P Time residual (sec)	0.038	0.025	0.251
P Velocity (km/sec)	5.947	5.357	5.371
P Azimuth (deg)	342.0	48.0	324.0
P Az residual (deg)	−9.2	27.2	−2.4
S Travel time (sec)	89.080	179.393	198.445
S Time residual (sec)	0.118	0.271	0.459
S Velocity (km/sec)	3.369	3.297	4.103
S Azimuth (deg)	349.0	49.0	335.0
S Az residual (deg)	−2.2	28.2	8.6

tions, in some cases exceeding 100 km (DREGER *et al.*, 1997). Table 1 lists the event locations, adopted as "ground truth" for comparison purposes, which were determined applying local data recorded by the Southern California Seismic Network (SCSN).

Calibration Event Analysis

Event #6 in Table 1, the largest event in the Ridgecrest sequence, was chosen as the calibration event for the purpose of calibrating the location procedure. For this analysis the SCSN location, given in Table 1, is adopted as "ground truth." The secondary P-wave and S-wave onset times for this event at the three broadband stations were measured and the results are given in Table 2. The corresponding wave azimuths were determined with the aid of Equation (2). Table 2 also supplies the absolute travel times, distances, great circle azimuths, and the inferred wave velocities for comparison. The wave velocities and the wave azimuths, relative to the great circle azimuth, vary considerably among the three stations. This variation is expected given the structural differences (see Fig. 1) along the propagation paths from Ridgecrest to the three stations. Interestingly, the largest wave propagation direction deviation is seen at ELK where the apparent propagation direction is ~28 degrees clockwise (CW) of the great circle path (of course this assumes that the ELK horizontal seismometers were properly aligned N and E). Upon closer inspection, the CW deviation from the great circle path is real and it is attributed to the lateral refraction of the wavefield along the high contrast boundary between the Sierra Nevada and the Basin and Range physiographic provinces (see Fig. 1) where the Sierra Nevada has the higher velocities. One might have expected the deviations to be the largest at YBH since the propagation path traverses three physiographic provinces as shown in Figure 1.

The "ground-truth" calibration event location and origin time were adopted and the phase arrival times at the three stations were determined and used to construct a 1-D linear gradient layer over a half-space velocity model, using a forward modeling approach, for each of the propagation paths and the onset time residuals were determined using these path-dependent models. Azimuth residuals relative to a great circle propagation path were also determined. These phase time and azimuth residuals were adopted as the corresponding station phase onset times and wave azimuth adjustments for locating the events. The path-dependent velocities, phase times and azimuth, and the corresponding phase and azimuth adjustments are given in Table 2. As a check on the location procedure, the calibration event was relocated using the path-dependent 1-D velocity models and the corresponding station phase arrival time and wave azimuth adjustments and the relocated epicenter were within 160 meters of the adopted "ground-truth" location as shown in Table 1. To determine the sensitivity of the calibration event solution to missing and or erroneous phase time and azimuth data, a series of tests were performed in which the phase times and azimuths were randomly omitted, the phase times were randomly perturbed by ± 1 second, and the wave azimuths were randomly perturbed by ± 1 degree. The resulting solutions were all within 8 km of the "ground-truth" location, and the corresponding P_{95} contour shape changed slightly as the data were omitted, and its size increased as the "mislocation" distance increased. This implies that the location procedure is quite robust and capable of locating regional events within the CTBT criteria. As a final test, the entire process was repeated using a single 1-D velocity model with corresponding phase and azimuth adjustments for each station. When the phase times and azimuths were randomly omitted, the phase times were randomly perturbed by ± 1 second, and the wave azimuths were randomly perturbed by ± 1 degree, the scatter in the solutions increased by about 15 percent over the path-dependent model results. The geological map shows both Quaternary volcanic flow rocks and Mesozoic granite in the vicinity of the Ridgecrest source region consequently the differences in the observed scatter between the two velocity models may be due to lateral structure in the source region.

Ridgecrest Sequence Analysis

The Ridgecrest sequence events in Table 1 were analyzed and located, systematically proceeding from the largest to the smallest M_L events. The path-dependent velocity models and phase time and wave azimuth adjustments derived from the calibration event, given in Table 2, were used in the location procedure and the results portrayed in terms of the "mislocation" distance from the "ground-truth" location are shown in Table 3 and Figure 7. The largest events, $M_L \geq 5$, generated the shortest mislocation distances (less than 3.6 km) and the "mislocation" distance increased as the event M_L decreased. This is as expected since the SNR decreases

Table 3

Event mislocation distances

Event #	M_L	Mislocation distance (km)	P_{95} radius (km)
1	5.4	0.3	3
2	4.2	7.2	4
3	4	6.9	4
4	3.9	13.7	11
5	4.2	1.9	4
6	5.8	0.16	0.045
7	3.9	9	15
8	3.9	11.9	16
9	4	3.6	6
10	4	6.2	7
11	3.7	9.5	18
12	3.6	9.8	20
13	3.5	16.4	24
14	5.2	3.6	4

proportionally with decreasing M_L. Note that the P_{95} average radius increases significantly below $M_L \sim 4$. This is because the phase time and wave azimuth data recorded at YBH and the wave azimuth data recorded at ELK were not well resolved, owing to degradation in the SNR. As discussed in the section on broadband waveform SNR, we expected the P-wave and S-wave SNR at YBH (800 km from Ridgecrest) to degrade to 0 dB at $M_L \sim 3.8$ and the wave azimuth data to be only moderately resolved below $M_L \sim 4.5$. Thus it is not surprising that the threshold M_L for reliably reading any body-wave phase data at YBH is approximately M_L 4. One inference is that the minimum SNR necessary to read phase times is ~4 dB. Also from the broadband waveform SNR analysis, the phase azimuth data at ELK

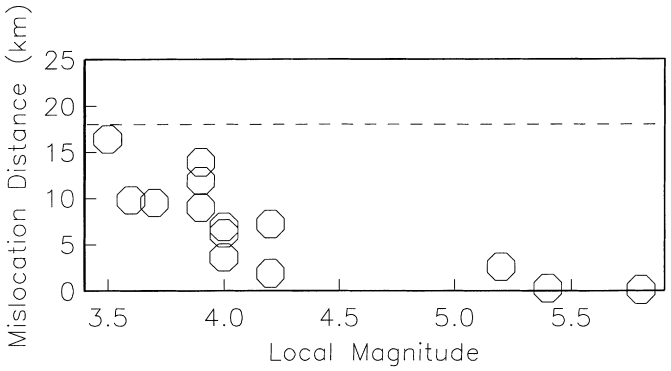

Figure 7

Event mislocation distance relative to the adopted "ground-truth" locations given in Table 1. The dashed line is the 18 km CTBT threshold. Note that the mislocation distance increases significantly below $M_L \sim 4$.

(600 km from Ridgecrest) will not be resolvable below a $M_L \sim 4$ threshold. This is consistent with the general increase in the "mislocation" distance and the P_{95} average radius below M_L 4, as shown in Table 3, and it is directly attributable to the omission of unreliable phase time and wave azimuth when determining the event location. Note that the "mislocation" distance (Table 3 and Figure 7) for all events is below the 18-km CTBT criteria. However, this does not insure that all the events are reliably located within the 18-km radius area. Note that the average P_{95} threshold radius is larger than ~15 km for most of the $M_L < 4$ events in Table 3 therefore the probability that these events are within the 18-km radius CTBT criteria can be considerably less than 95 percent. For example, event #13 has a "mislocation" distance of 16.4 km and a P_{95} average radius of 24 km consequently there is only a 43 percent probability that it is actually located within the 18-km radius region.

Conclusions

We have introduced the *BW_RELP* location algorithm and demonstrated its performance using data from a sparse three-station regional network of three-component broadband seismic stations, to locate events in the 1995 Ridgecrest earthquake sequence. *BW_RELP* employs an adaptive migrating grid search algorithm to locate the hypocenter by finding the global minimum in a misfit parameter. The algorithm was specifically designed to utilize more of the information inherent in broadband seismic recordings, by using both phase onset times and wave azimuth data to locate events. It is very flexible in that it allows for path-dependent velocity models, station adjustments, and azimuth adjustments. Also the algorithm has no default parameter values, and the user must supply all the required parameter values. This was done deliberately as appropriate parameter values are not necessarily obvious *a priori*. The adaptive grid search procedure is also more amenable to the incorporation of 3-D velocity models because it is not necessary to compute complicated partial derivatives. Unlike conventional linearized least-squares algorithms, *BW_RELP* also makes no assumptions regarding the shape of the error surface and it provides more robust parameter uncertainty estimates, especially when using data from a sparse network to locate distant events.

The results of our analysis of the Ridgecrest sequence reveal that it is indeed possible to resolve event locations with an accuracy bettering 18 km, as prescribed by the CTBT, when using a sparse three-station network of regional distance (300–800 km) broadband, three-component seismic stations. Achievement of this degree of accuracy requires the availability of an appropriate event to calibrate the location procedure. Without a calibration event, the "mislocation" distances can be quite large, often exceeding 100 km. The primary advantages of a calibration event are that it provides a template for phase selection and cross-correlation and a "ground-truth" location to determine appropriate path-dependent velocity models and phase

arrival time and wave azimuth adjustments. With appropriate selection of the seismic phases and wave azimuths to measure for use in the location algorithm, we find that all three broadband stations in the sparse network provide useful data for locating the Ridgecrest events down to a $M_L \sim 4$ threshold. The limiting factors are the SNR and the intrinsic attenuation/scattering along the seismic wave propagation path.

Below $M_L \sim 4$, the events can be located with reduced accuracy, by omitting phase arrival time and wave azimuth from the farthest (YBH, 800 km distant) and also wave azimuth data from the next most distant station (ELK, 600 km distant), down to $M_L \sim 3.5$. Consistency in the determination of the phase arrival time and wave azimuth picks is paramount to achieving the most reliable relative event locations. We find that secondary P-wave arrivals (Pg, for example) are consistently observed over a wider M_L range, than are the primary P-wave arrivals, and with appropriate filtration of the broadband seismic signals they can be reliably measured as long as the SNR is more than $\sim$4 dB for measuring the arrival time and exceeds $\sim$12 dB for measuring wave azimuth. Below these thresholds the accuracy degrades rapidly, and it is better to omit the data than to chance biasing the solution with unreliable observations.

Acknowledgements

This work was partially supported by the Lawerence Livermore National Laboratory, through the Department of Energy's Comprehensive Test-Ban-Treaty Research and Development (CTBT R & D) Program, under the Inter-University (IU) Agreement No. B331608. The data used in this work were acquired from the Northern California Earthquake Data Center (NECDE; http://quake.geo.berkeley.edu), the Southern California Earthquake Data Center (SCEC_DC; http://scecdc.scec.org), and the IRIS DMC (http://www.iris.washington.edu). This is Berkeley Seismological Laboratory contribution 00-03.

References

Buland, R. (1976), *The Mechanics of Locating Earthquakes*, Bull. Seismol. Soc. Am. *66*, 173–187.

Dreger, D., and Romanowicz, B. (1994), *Source Characteristics of Events in the San Francisco Bay Region*, USGS Open-File Report *94–176*, 301–309.

Dreger, D., Pasyanos, M., Uhrhammer, R., Romanowicz, B., and Ryall, A. (1996), *Evaluation of the performance of broadband networks and short-period arrays in global monitoring*, Proceedings of the 18th Annual Seismic Research Symposium on Monitoring a CTBT, *PL-TR-96-2153*, 704–713.

Dreger, D., Pasyanos, M., Uhrhammer, R., Franck, J., and Romanowicz, B., (1997), *Evaluation of the Performance of Broadband Stations and Regional Arrays in Global Monitoring – Phase II*. Final Report, submitted July 1997, 10 pp.

Flinn, E. A. (1965), *Confidence Regions and Error Determinations for Seismic Event Location*, Rev. Geophys. *3*, 157–185.

GEIGER, L. (1910), *Herdbestimmung bei Erdbeden aus den Ankunftzeiten*, K. Gessel. Wiss. Goett. *4*, 331–349.

KENNETT, B. L. N., *Event location and source characterization*. In *Monitoring a Comprehensive Test Ban Treaty* (E. S. Husebye and A. M.Dainty, eds.) (Kluwer Academic Publishers, 1996) pp. 501–520.

LEE, W. H. K., and LAHR, J. C. (1972), *HYPO71: A Computer Program for Determining Hypocenter, Magnitude, and First Motion Pattern of Local Earthquakes*, U.S. Geol. Survey, Open File Report 72–0224.

SAMBRIDGE, M. S., and KENNETT, B. L. N. (1986), *A Novel Method of Hypocenter Location*, Geophys. J. Royal astr. Soc. *87*, 679–697.

TARANTOLA, A., and VALETTE, B. (1982), *Generalized Nonlinear Inverse Problems Solved Using the Least-squares Criterion*, Rev. Geophys. and Space Phys. *20*, 219–232.

(Received July 20, 1999, revised August 3, 2000, accepted September 3, 2000)